Sliding Mode Control of Feed Drive System for a three-axis Micro-Machining Platform with Nano-Resolution

Yingfeng Ji, *Chengying Xu

Mercedes-Benz Research and Development, North American, Inc, Detroit, MI

Department of Mechanical and Aerospace Engineering, University of Central Florida, Orlando, US

Email: yji929@gmail.com

* Corresponding author. Email: cxu@mail.ucf.edu

***Abstract*- The feed drive system plays a key role of increasing processing efficiency and improving machining quality of parts. The external disturbances, such as cutting forces and frictional nonlinearities seriously affect the machining quality. The feed drive system should be capable of rejecting such disturbances. In this paper, the feed drive system of a micro-machining platform with nano-resolution was modeled and controlled. A decoupled algorithm was implemented to linearly regulate flux-producing and force-producing currents of motor. The current controller was designed based on the electrical model of motor employing pole-zero cancellation method. The speed controllers, i.e., proportional-integral (PI) and sliding mode control (SMC) were designed and compared. The SMC exhibits the better property of rejecting the external disturbance compared to PI controller. The electromagnetic force produced by Linear Permanent Magnet Synchronous Machine (LPMSM) under SMC expresses the quicker response to external variations. The models will be further applied for the design of cross-coupling servo control for this five-axis reconfigurable micro-machining platform.**

Keywords- Sliding Mode Contro;Micro-Maching; Nano-Resolution

I. INTRODUCTION

Linear permanent magnet synchronous machines (LPMSM) are employed in many industrial fields due to the inherent merits: simple structure, less friction, zero backlash and maintenance free [1, 15, 16]. LPMSMs are utilized in micro-machining to provide the actuation for feed drive system. However the performance of feed drive system is often degraded by the external disturbances, such as cross-coupling dynamics and cutting forces. Therefore it is greatly significant to develop the dynamic models of a specific feed drive system for the improvement of control algorithms and the optimization of the overall feeding system. Our overall objective is to re-equip a commercial three-axis micro-machining platform to a five-axis reconfigurable system. Such a system serves as a universal platform for advanced material machining [11-13], biological cell handling, micro assembly, inspection of an integrated circuit [14], etc.

In this paper, we only focus on modeling and control of feed drive system for further investigation on this proposed five-axis micro-machining system.The existing feed drive system is composed of a three-axis (X, Y, Z) linear stage and an Aerotech Ensemble multi-axis motion controller as shown in Figure 1. The proposed five-axis reconfigurable system will be introduced another two rotary axes actuated by Aerotech motors. The Advanced Motion Controller (DPRAHIS-015A400) and related systematic components were employed in the new system. The micro-machining machine is set up on a tetrahedral space frame.

The air-bearing spindle (NSK E800Z) is fixed at the center of the tetrahedral frame. The highest speed of the spindle is 8×104 rpm. A Kistler 9256C2 piezoelectric dynamometer is used to measure cutting forces. The vibration of the machining tetrahedral platform is measured by a PCB piezoelectric ICP accelerometer, which is mounted at the spindle holder. The control platform is based on NI PXI-1042Q installed the NI PXI-7854R for Labview real-time FPGA target application. Each of feed drive axes includes a LPMSM. The position resolution of the LPMSM is 4 nm for X and Y axes, and 9 nm for Z axis. The model of LPMSM is BLMUC-95 for X, Y axes and BLMUC-79 for Z axis. The mover (rotor) of LPMSM is magnetic track and the stator is winding coils. Each of two rotational axes will be equipped with a rotary PMSM.

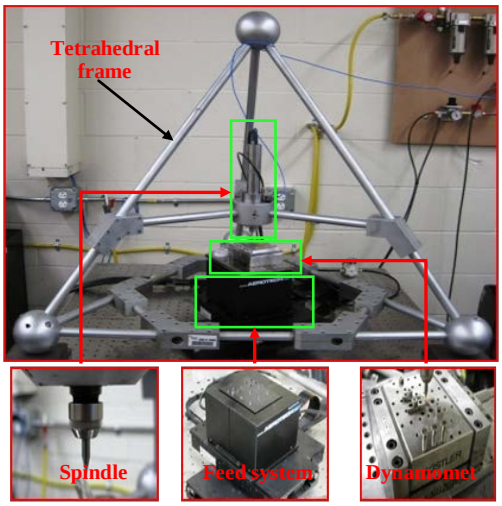

Figure 1: Micro-machining system

We developed the dynamic models and control algorithms for a linear feed drive system based on vector (field-oriented) control methodology in this paper. Precise velocity regulation is the base of position and cross-coupling

control which governs the dimensional accuracy of machined parts, especially for micro-machining. The speed control algorithms for improving the capability of external disturbance rejection were developed. Several functional models for feed drive system were developed including d-q dynamic model of LPMSM, transformation models and Space Vector Pulse-Width Modulation (SVPWM). The architecture of servo system is illustrated in Figure 2. The symbols vr, iqr and idr are the reference inputs for velocity, force-producing current and flux-producing current, respectively. The current idr usually is set up to zero for PMSM. The symbols sm and se are mechanical and electrical displacements of motor. Tm-e is the transformation function. The symbols Gcv, Gcdi and Gcqi are the velocity, flux-producing current and force-producing current controllers, respectively. The voltages and currents such as Vd, Vq, id and iq in rotating coordinate are independent on mover position. The variables in stationary coordinate α-β and a-b-c are time-varying at the same frequency which is dependent on the velocity of motor.

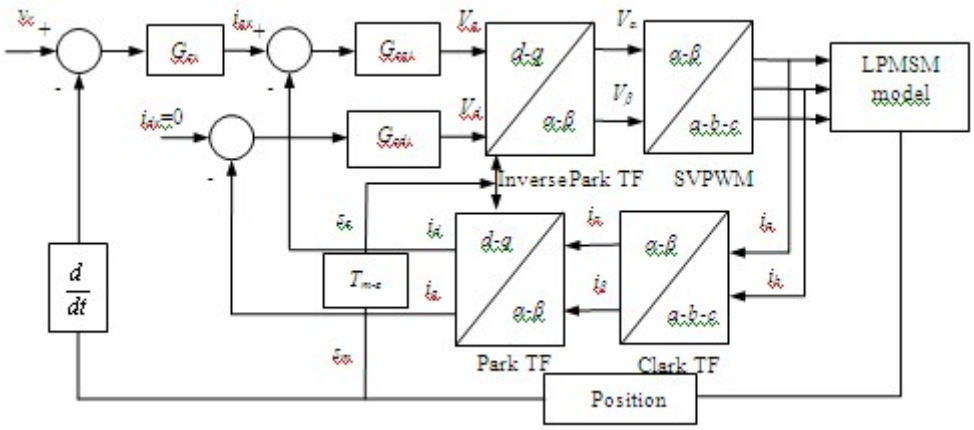

Figure 2: Velocity-current *d*-*q*servo control scheme

In this paper, a linear feed drive system for micro-machining platform was systematically modeled. The current and velocity controllers were designed and evaluated. The remainder of this paper is organized as follows. In Section II, vector control is introduced, and the model of LPMSM is presented. SVPWM is explained and modeled. In Section III, the controllers are designed and the decoupling feed forward compensations are described. In Section IV, the results are presented and discussed. Section V, the conclusions are obtained and the future work is pointed out.

II. DYNAMICS MODELING OF FEED DRIVE SYSTEM

A. *Modeling of LPMSM*

Field-oriented control, also called vector control, can achieve a better dynamic response for motor control. To implement it, a series of coordinate transformations are necessary as shown in equations (1-4) based on Figure 3. The purpose of coordinate transformations is to transfer three-phase dependent variables in a-b-c coordinate (stator) to two independent scalars in d-q coordinate (mover). For a given reference vector, e.g., current I in Figure 3, it can be transformed from three-phase a-b-c coordinate to two-phase α-β based on equations (1-2) under the condition of ia+ib+ic=0. Equations (3-4) can be used to transform α-β coordinate to d-q frame. The transformations are usually known as Clark and Park transformations, respectively [2]. The inverse Clark and Park transformations can be easily derived as required.

$$i_\alpha = i_a \tag{1}$$

$$i_\beta = \frac{1}{\sqrt{3}} i_a + \frac{2}{\sqrt{3}} i_b \tag{2}$$

$$i_d = i_\alpha \cos\theta_e + i_\beta \sin\theta_e \tag{3}$$

$$i_q = i_\beta \cos\theta_e - i_\alpha \sin\theta_e \tag{4}$$

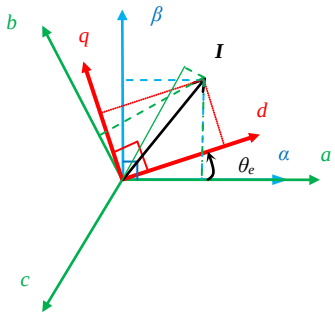

Figure 3: Coordinate transformations

To develop the dynamic model in rotational coordinate (d-q) for LPMSM, some assumptions regarding to this motor have to be emphasized. The mover flux due to the permanent magnet was thought to constantly exert along d axis. Motor core, hysteresis and eddy current losses were negligible.

Variations of mover (magnet) flux with respect to temperature and time were not considered. The equivalent circuits in d-q axes can be referred to Figures 4-5, respectively [3]. The mover flux coincides with d axis. The dynamic models can be expressed as follows:

$$V_q = R_q i_q + L_q \frac{di_q}{dt} + \frac{\pi}{d} v_e L_d i_d + \frac{\pi}{d} v_e \psi_{PM} \tag{5}$$

$$V_d = R_d i_d + L_d \frac{di_d}{dt} - \frac{\pi}{d} v_e L_q i_q \tag{6}$$

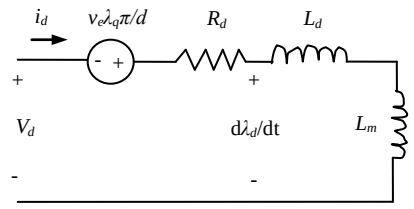

Figure 4: LPMSM equivalent circuit of *d*-axis

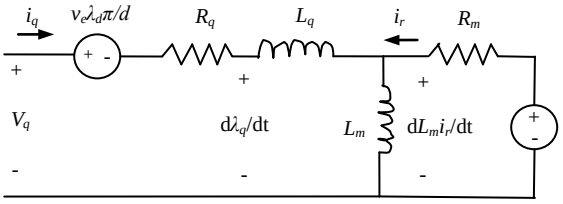

Figure 5: LPMSM equivalent circuit of *q*-axis

This dynamic model in d-q reference frame will be linearized through decoupled feedforward compensations illustrated in Section III. For the surface-mounted PM machine, the inductance in direct axis L_d is equal to the inductance in quadrature axis L_q. The electromagnetic force produced by LPMSM can be generalized as follow:

$$\begin{aligned} F^e &= \frac{3}{2}\frac{\pi}{d}[L_m i_{dr} i_q + (L_d - L_q) i_q i_d] \\ &= \frac{3}{2}\frac{\pi}{d}\psi_{PM} i_q = K_f i_q \end{aligned} \tag{7}$$

The mechanical linear velocity can be calculated as:

$$v_m = \frac{2v_e}{p} \tag{8}$$

where V_d, V_q, i_d, i_q, λ_d, λ_q, R_d, R_q, L_d, L_q are voltages, currents, flux linkages, winding resistances and inductances for *d* and *q* axes, respectively. L_m and R_m represent mutual inductance and resistance between stator winding and mover magnet. i_r is equivalent current in *d* axis due to mover (rotor) magnet. *p* represents pole number. v_e and v_m are electrical and mechanical linear velocities, respectively. *d* denotes pole pitch of magnet track. ψ_{PM} is flux linkage due to permanent magnet. k_f, F^e and θ_e represent force constant, electrical force and angular displacement of PM flux linkage, respectively.

The governing equation of mechanical dynamics related to the electromagnetic forces can be represented as:

$$F^e = M\dot{v}_m + Bv_m + F_l + F_d \tag{9}$$

where*M* is the mass of mover. *B* represents the damping coefficient of system. F_l, F_d represent load and external disturbance, respectively.

B. Modeling of SVPWM

This modulation method transforms the variables in stationary coordinate (*α-β*) to the PWM signals which control the switches (S_1~S_6) of power inverter shown in Figure 6 [8]. The three-phase pseudo sinusoidal currents are produced for motor windings utilizing DC-bus voltage V_{dc}. This method produces less harmonic distortions and utilizes the voltage of DC-bus more efficiency than sinusoidal modulation technique. The symbols L_s and R_s represent the inductance and resistance of phase windings of motor. When the inverter works, three of six switches must always be ON and the other three ones are always OFF. The upper and lower switches of the same leg are on complementary pulsed signals.

The combination of ON/OFF states in power inverter for switches S_1~S_6 is coded by three-digit number (000~111). Each digit bit represents one phase. The "1" means that the upper switch is ON and the bottom switch is OFF. The "0" means that the upper switch is OFF and the bottom one is ON.

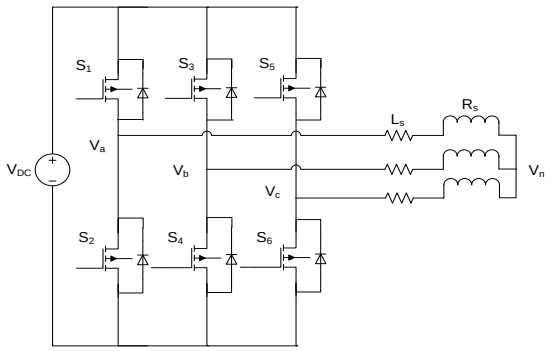

Figure 6 Illustrative diagram of three-phase power inverter

The principle of producing PWM signals is called SVPWM which is explained in Figure 7 [8]. The reference voltage $\mathbf{V}_{ref}$ can be synthesized by two adjacent vectors and two zero vectors. These reference vectors need to function for a certain time period. Six non-zero reference vectors are $\mathbf{V}_1$(100), $\mathbf{V}_2$(110), $\mathbf{V}_3$(010), $\mathbf{V}_4$(011), $\mathbf{V}_5$(001) and $\mathbf{V}_6$(101). Two zero reference vectors are $\mathbf{V}_0$(000) and $\mathbf{V}_7$(111). When reference voltage $\mathbf{V}_{ref}$ is located in sectors I, II, III, IV, V or VI, the switching sequence of reference vectors is shown in Figure 7. The switch states for 8 reference vectors are shown in Figure 8. Table 1 shows the values of V_a, V_b, V_c, V_α and V_β for 8 reference vectors.

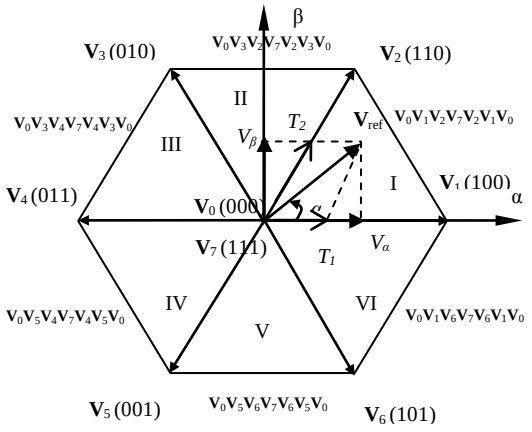

Figure 7: Illustrative diagram of 8 vectors and 6 sectors

Assuming reference voltage $\mathbf{V}_{ref}$ is located in sector I, the conduction time of reference vectors is governed by the vector equations (10-11). An illustrative graph of time distribution in a PWM signal circle can be referred to Figure 9. The detail theory of calculating the T_1, T_2 and $T_0$is explained in [4].

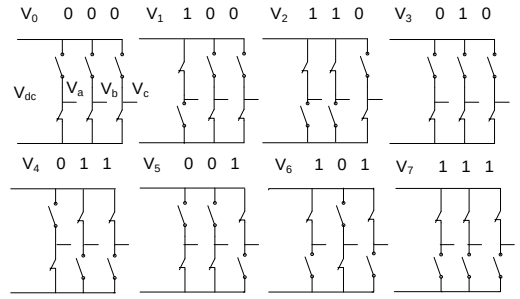

Figure 8: Illustrative diagram of switch states for 8 vectors

$$\mathbf{V}_{ref}T_{PWM} = \mathbf{V}_1T_1 + \mathbf{V}_2T_2 + \mathbf{V}_0T_0/2 + \mathbf{V}_7T_0/2 \quad (10)$$

$$T_{PWM} = T_1 + T_2 + T_0 \quad (11)$$

where T_1, T_2, T_0 are the conduction time of vector $\mathbf{V}_1$, $\mathbf{V}_2$ and zero vectors $\mathbf{V}_0$, $\mathbf{V}_7$. T_{PWM} is the period of PWM signal.

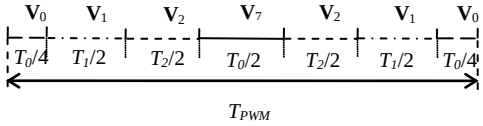

Figure 9: Time distribution of a PWM circle when $\mathbf{V}_{ref}$ is located in sector I

To produce the $\mathbf{V}_{ref}$ for motor windings, it is fundamental to know the sectors where $\mathbf{V}_{ref}$ is located so that the two corresponding non-zero vectors can be known. The sector number can be calculated based on the information of the angle which can be found through equation (12) [4]:

$$\alpha = \arctan(\frac{V_\beta}{V_\alpha}) \quad (12)$$

Table 1: Values of V_a, V_b, V_c, V_α, V_β of 8 reference vectors

Vectors	Va	Vb	Vc	V_α	V_β
$\mathbf{V}_0$	0	0	0	0	0
$\mathbf{V}_1$	$2V_{dc}/3$	$-V_{dc}/3$	$-V_{dc}/3$	$2V_{dc}/3$	0
$\mathbf{V}_2$	$V_{dc}/3$	$V_{dc}/3$	$-2V_{dc}/3$	$V_{dc}/3$	$\sqrt{3}V_{dc}/3$
$\mathbf{V}_3$	$-V_{dc}/3$	$2V_{dc}/3$	$-V_{dc}/3$	$-V_{dc}/3$	$\sqrt{3}V_{dc}/3$
$\mathbf{V}_4$	$-2V_{dc}/3$	$V_{dc}/3$	$V_{dc}/3$	$-2V_{dc}/3$	0
$\mathbf{V}_5$	$-V_{dc}/3$	$-V_{dc}/3$	$2V_{dc}/3$	$-V_{dc}/3$	$-\sqrt{3}V_{dc}/3$
$\mathbf{V}_6$	$V_{dc}/3$	$-2V_{dc}/3$	$V_{dc}/3$	$V_{dc}/3$	$-\sqrt{3}V_{dc}/3$
$\mathbf{V}_7$	0	0	0	0	0

III. CONTROLLERS AND DECOUPLING DESIGN

A. Current Controller Design

The direct-axis stator current and quadrature-axis current must be controlled independently. The stator voltage equations (5-6) in d-q frame need to be decoupled. Then the Vd and Vq are independently controlled by controlling the terminal voltages of motor. The equations (5-6) can be reformulated to linear parts and decoupled terms as follows [9]:

$$V_{linear}^q = R_q i_q + L_q \frac{di_q}{dt} \quad (13)$$

$$V_{linear}^d = R_d i_d + L_d \frac{di_d}{dt} \quad (14)$$

$$V_{decoupled}^q = \frac{\pi}{d} v_e L_d i_d + \frac{\pi}{d} v_e \psi_{PM} \quad (15)$$

$$V_{decoupled}^d = -\frac{\pi}{d} v_e L_q i_q \quad (16)$$

This decoupling method transforms nonlinear model to linear model in equations (13-14) where current controllers were designed. The cross-coupling terms in equations (15-16) are compensated. For surface-mounted PMSM, the current controllers are same for d and q axes loops. The delays of A/D and SVPWM inverter were neglected. A PI controller is in the style of equation (17). The transfer function of motor in d axis is expressed as equation (18). Therefore the closed-loop transfer function can be derived as shown in equation (19).

$$G_c(s) = k_p + k_i / s \quad (17)$$

$$G_p(s) = \frac{1}{L_d s + R_d} \quad (18)$$

$$G(s) = \frac{\frac{k_p}{L_d}s + \frac{k_i}{L_d}}{s^2 + (\frac{k_p + R_d}{L_d})s + \frac{k_i}{L_d}} \quad (19)$$

The PI controller introduces a left hand side zero to closed-loop. This will increase the system overshoot and lower the closed-loop bandwidth. A zero cancellation transfer function [5] with unit gain was added to closed-loop as follow:

$$G(s) = \frac{\frac{k_i}{k_p}}{s + \frac{k_i}{k_p}} \cdot \frac{\frac{k_p}{L_d}s + \frac{k_i}{L_d}}{s^2 + (\frac{k_p + R_d}{L_d})s + \frac{k_i}{L_d}} \quad (20)$$

The current PI controller was designed through comparing closed-loop transfer function with standard second order transfer function in equation (21). Therefore the controller gains kp and ki can be designed as shown in equations (22-23) according to the specific requirements.

$$G_s(s) = \frac{k\omega_n^2}{s^2 + 2\xi\omega_n s + \omega_n^2} \quad (21)$$

$$k_p = 2\xi\omega_n L_d - R_d \quad (22)$$

$$k_i = \omega_n^2 L_d \quad (23)$$

B. Speed Controller Design

Comparing to current loop, the parameters of plant model in speed loop are usually difficult to determine. The systematic lumped mass is changed and mechanical load on motor is variable and unpredictable, such as the cutting force

and other external disturbances. The speed controller should be capable of rejecting the disturbances and handling with the modeling uncertainties. The speed control block diagram is as follow:

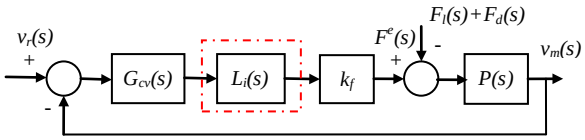

Figure 10: Illustrative diagram of speed control

The $v_r(s)$, $v_m(s)$ are reference speed input and actual speed output. $G_{cv}(s)$ is speed controller. We will design two types of speed controllers. One is the PI speed controller which is in the type of:

$$G_{cv}(s) = k_{vp} + k_{vi}/s \tag{24}$$

Another is the SMC as shown in equation (33). $L_i(s)$ inside dashed red square represents vector control current loop.

Since mechanical time constant is greater than electrical time constant, speed loop is sampled slower than current loop [6]. Electrical and mechanical time constants in this paper are 0.00135 and 0.1357, respectively. The delays due to current loop were neglected during speed controller design. $P(s)$ is the model of mechanical dynamic in motor system.

$$P(s) = \frac{1}{Ms + B} \tag{25}$$

The characteristic equation is as follow:

$$Ms^2 + (k_{vp}k_f + B)s + k_{vi}k_f = 0 \tag{26}$$

The speed PI controller can be designed according to the desired damping coefficient and natural frequency shown as follows [5]:

$$\xi_v = \frac{k_{vp}k_f + B}{2\sqrt{Mk_{vi}k_f}} \tag{27}$$

$$\omega_{nv}^{\ 2} = k_{vi}k_f / M \tag{28}$$

A sliding mode speed controller was designed to compare with the performance of PI speed controller. To design the sliding mode speed controller, the tracking error is firstly defined as $e=v_r-v_m$. The sliding surface can be designed as $s = \dot{e} + ce$. The symbol c is non-negative constant which guarantees the tracking error converges to zero when the states reach the sliding surface.

Based on equation (9) and inverse Laplase transformation, the dynamic system can be expressed as follow:

$$sV_m(s) = \frac{k_f}{M}I_q(s) - \frac{B}{M}V_m(s) - \frac{1}{M}F_l(s) \tag{29}$$

Considering the q axis current controller G_{cqi} in Figure 2, the relationship between q axis voltage $V_q(s)$ and reference current $I_{qr}(s)$ can be derived as [7]:

$$\frac{V_q(s)}{I_{qr}(s) - I_q(s)} = k_p + \frac{k_i}{s} \tag{30}$$

Combining equations (29-30) and implementing the inverse Laplace transformation, assuming the initial conditions are zeros, a key equation can be obtained:

$$\ddot{v}_m + (\frac{B}{M} + \frac{k_i}{k_p})\dot{v}_m + \frac{B \cdot k_i}{M \cdot k_p}v_m = \frac{k_f}{M}(\dot{i}_{qr} + \frac{k_i}{k_p}i_{qr}) + d(t) \tag{31}$$

where $d(t)$ is treated as a disturbance as follow:

$$d(t) = -\frac{k_f}{M \cdot k_p}\dot{V}_q - \frac{1}{M}(\dot{F}_l + \frac{k_i}{k_p}F_l)$$

Taking double derivative of tracking error and submitting into equation (31), we can have:

$$\ddot{e} = \ddot{v}_r + (\frac{B}{M} + \frac{k_i}{k_p})\dot{v}_m + \frac{B \cdot k_i}{M \cdot k_p}v_m - \frac{k_f}{M}(\dot{i}_{qr} + \frac{k_i}{k_p}i_{qr}) - d(t) \tag{32}$$

On sliding surface, the error dynamics ($\ddot{e} + c\dot{e} = 0$) is satisfied. The control input terms can be expressed as equation (33) based on the definition of sliding mode control [10] to achieve the convergence to the sliding surface.

$$\frac{k_f}{M}(\dot{i}_{qr} + \frac{k_i}{k_p}i_{qr}) = c\dot{e} + \ddot{v}_r + (\frac{B}{M} + \frac{k_i}{k_p})\dot{v}_m + \frac{B \cdot k_i}{M \cdot k_p}v_m + K \cdot sat(s/\Phi) \tag{33}$$

The constant K is a gain to guarantee that all the trajectories outside the boundary layer are attracted toward the boundary. The symbol $sat(s/\Phi)$ represents linear saturation function which would be defined as follows:

$$|s/\Phi| \le 1,\ sat(s/\Phi) = s/\Phi$$

$$|s/\Phi| > 1, \text{ if } s/\Phi > 1,\ sat(s/\Phi) = 1$$

$$\text{if } s/\Phi < -1,\ sat(s/\Phi) = -1$$

In order to satisfy sliding condition, a Lyapunov function $V = \frac{1}{2}s^2$ is defined. Its derivative is follow:

$$\begin{aligned} \dot{V} &= s\dot{s} = s[c\dot{e} + \ddot{e}] = s[-K \cdot sat(s/\Phi) - d(t)] \\ &\le -K|s| + |d(t)||s/\Phi| = -[K - |d(t)|]|s/\Phi| \end{aligned} \tag{34}$$

Assuming that the disturbance $d(t)$ is bounded:

$$|d(t) \le \delta| \text{ for } t \ge 0 \tag{35}$$

If $K > \delta$ in equation (34), then $\dot{V} \le 0$, the sliding condition is satisfied and stability is guaranteed. The state variables such as speed error reaches sliding surface $s=0$ during the finite time. After the state arrive at sliding surface, system dynamic will be governed by $s = \dot{e} + ce = 0$ and the speed error will converge to zero. To avoid the chattering effect in SMC, the saturation function is used to replace the signum function. A switching gain K is selected to be enough big to control the lumped disturbance $d(t)$.

IV. RESULTS AND DISCUSSION

The direct and quadrature current controllers were firstly designed based on equations (22-23). Then the PI and SMC speed controllers were developed according to equations (27-28, 33). The nominal parameters of LPMSM system are listed

in Table A of Appendix. Figure 11 is the overall simulink model in simulation processing. The load F_l in equation (9) was set up to 5 N, and the disturbance F_d is assumed as a step function with amplitude 20 N introduced at 0.1 second. The proportional and integral gains of PI current controller for both direct and quadrature axis are 20 and 1750. The velocity command is a step input with a 0.5 m/s amplitude. The DC-bus voltage is 80 Volt. The PWM duty circle is 0.0005 second. The simulation time is 0.2 second, but the simulation time is set up to 0.05 second in order to have the clearer plots in Figures 19-20. The simulation results from Figures 12-19 show the comparisons between traditional PI speed controller and sliding mode speed controller.

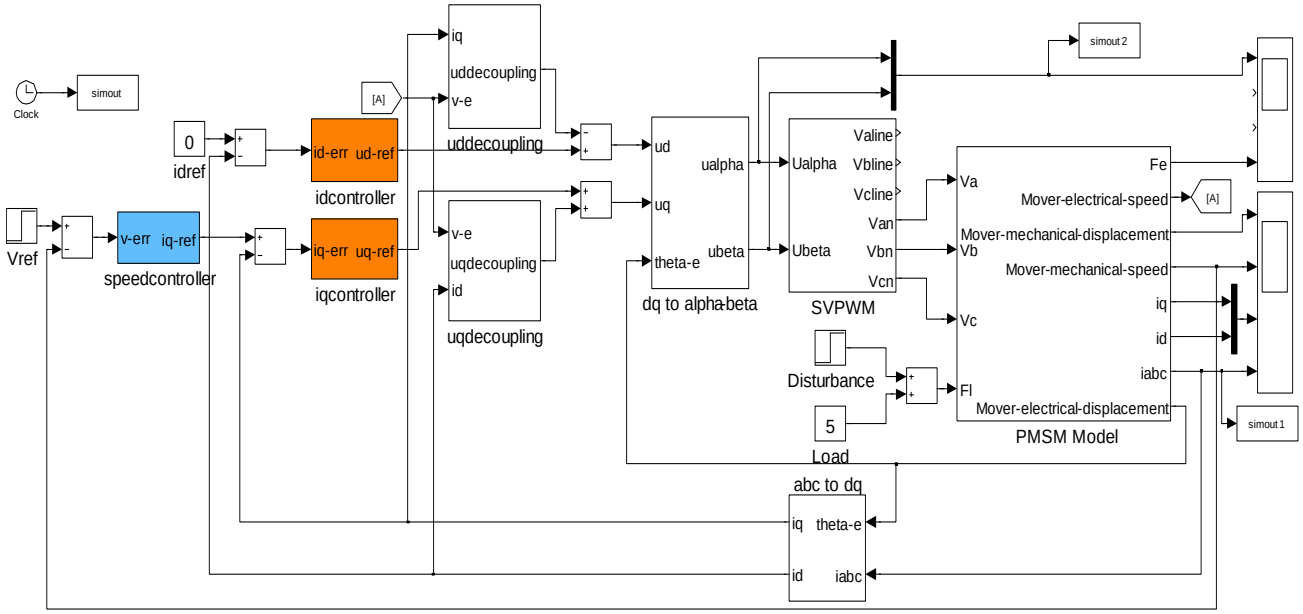

Figure 11: Simulinkmodel for this feed drive system

Figure 12 shows the details of speed responses under PI and SMC. The percentage overshoots are 6.28% for SMC, 1.4% under PI controller. The PI expresses the quicker response with settling time 0.0369 second, rising time 0.0149 second while SMC has a 2% settling time 0.0586 second and rising time 0.0204 second. However the PI controller performs a 0.033 m/s steady state error due to the external disturbance while the speed response under SMC was not affected by this external disturbance. SMC exhibits the excellent performance of rejecting the external disturbance. This is significantly important for the Micro-machining processing where the external disturbances, such as cutting forces and unexpected frictions are obviously predominant.

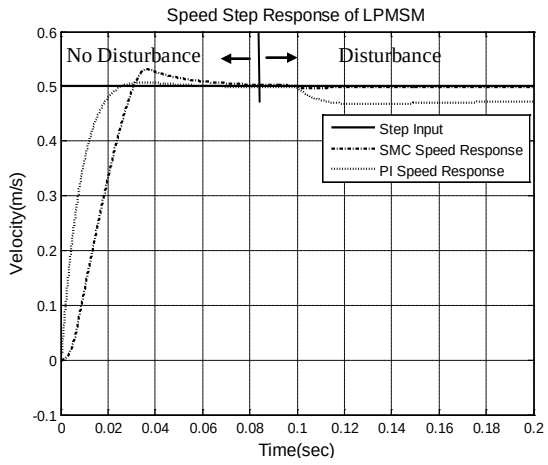

Figure 12: Velocity step response under PI and SMC

Even the slower speed response expressed by SMC, the LPMSM displacements under SMC and PI are close, e.g., 0.0925m and 0.0936m, respectively at 0.2 second as shown in Figure 13. This is contributed to the capability of rejecting the external disturbance for SMC.

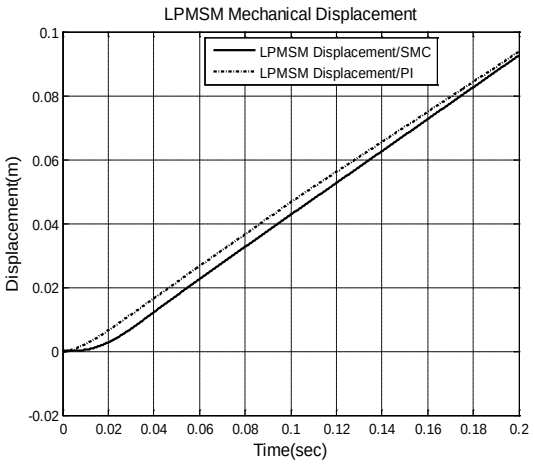

Figure 13: LPMSM linear displacement

The PI speed controller provides the quicker transient response, however the motor has to supply the bigger currents. In Figure 14, the maximum values of quadrature currents for PI case and SMC situation are 6.035A and 2.361A during the transient period. The corresponding currents in stationary coordinates (α-β and a-b-c) are bigger for PI controller case during the transient period as shown in Figures 15-16.

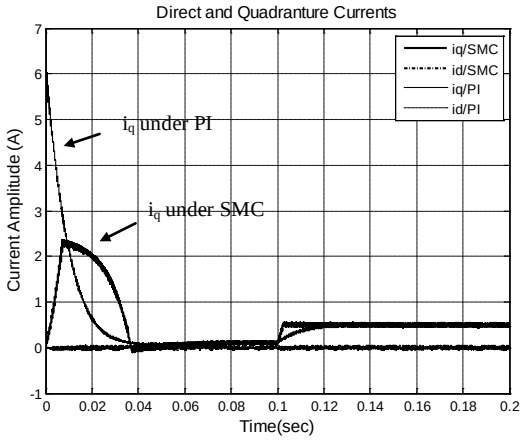

Figure 14: Scalar currents i_q and i_d under PI and SMC

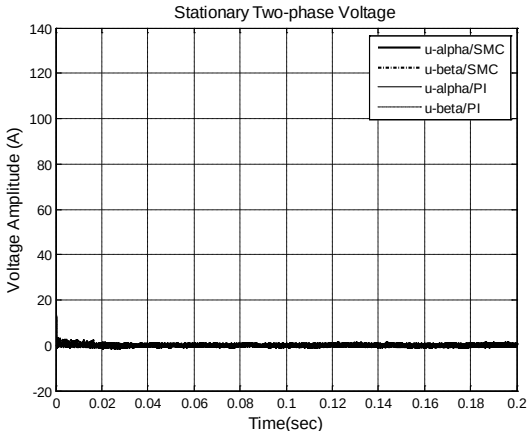

Figure 15: Stationary two-phase currents i_α and i_β under PI and SMC

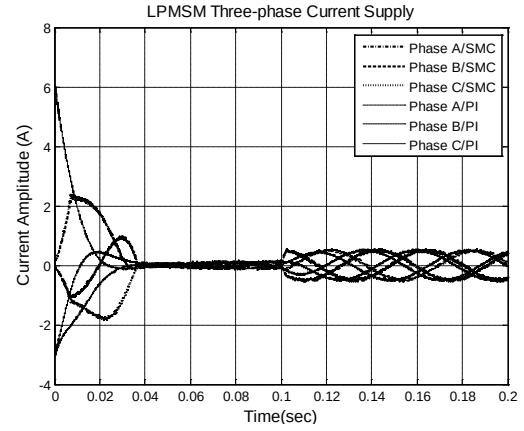

Figure 16: Stationary three-phase currents i_a, i_b and i_c under PI and SMC

Figure 17 shows the rotational displacement of flux linkage of permanent magnet. This variable is employed for the coordinate transformation between *d-q* frame and *α-β* coordinate. The electromagnetic force produced by motor is plotted in Figure 18. The trends of forces are consistent with i_q currents. The produced electromagnetic force exhibits a quicker response to external disturbance under the SMC. The sliding surface is shown in Figure 19.

The saturation function was not used to limit the current outputs in this paper. Therefore the peak values of the currents and forces during transient period are extremely high. This situation can be improved by the windup limitation in practical application.

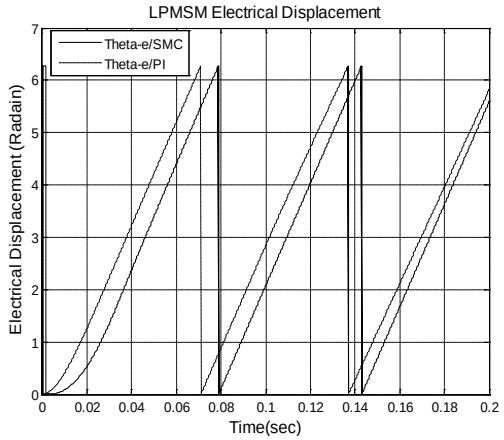

Figure 17: LPMSM rotational displacement of rotor flux linkage

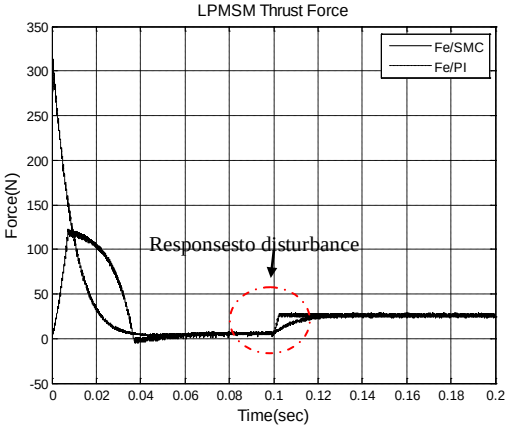

Figure 18: Electromagnetic forces produced by LPMSM under PI and SMC

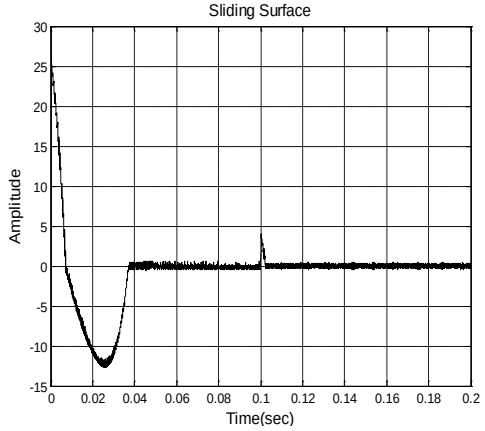

Figure 19: Sliding surface of SMC

V. CONCLUSIONS AND FUTURE WORK

In this study, the feed drive system of micro-machining platform was modeled and controlled. The direct drive system should be capable of rejecting the dynamic disturbance. A SMC algorithm comparing with the traditional PI controller was developed and verified. The results show that the SMC is highly capable of rejecting the external disturbance and keep the system stable. But the speed response is slower than the PI case. The future work will focus on the improvement of response speed and develop the parameters identification of mechanical system. We will configure the 5-axis micro-machining system and implement

the friction compensation for each of axes. The cross-coupling control among 5 axes will be considered in the future.

REFERENCES

Tam, M.S.W.; Cheung, N.C.; 2004, "A Robust Fully Digital Drive for Linear Permanent Magnet Synchronous Motor", Proceeding of International Conference on Power Electronics Systems and Applications, pp. 188-193.

Salaet, J.; Busquets, S.; Bordonau, J.; Alepuz, S.; 2006, "A New Strategy for Decoupling Direct and Quadrature Currents in a Rotating Frame Current Regulator Application to a Single-Phase Three-Level Boost Rectifier", IEEE Power Electronics Specialists Conference, pp. 1-7.

R. Krishnan, 2001, Electric Motor Drives-Modeling, Analysis and Control, Englewood Cliffs, NJ: Prentice Hall

K. Vinoth Kumar, Prawin Angel Michael, Joseph P. John and S. Suresh Kumar, 2010, "Simulation and Comparison of SPWM and SVPWM Control for Three Phase Inverter", Journal of Engineering and Applied Science, Vol. 5, pp. 61-74.

Pragasen Pillay, Ramu Krishnan, 1990, "Control Characteristics and Speed Controller Design for a High Performance Permanent Magnet Synchronous Motor Drive", IEEE Transactions on Power Electronics, Vol. 5, pp. 151-159.

Balazovic, P., Filka, R., 2008, "Sensorless PMSM Control for H-axis Washing Machine Drive", Power Electronics Specialists Conference, pp. 4237-4242.

Shihua Li, Kai Zong and Huixian Liu, 2010, "A composite speed controller based on a second-order model of permanent magnet synchronous motor system", Transactions of the Institute of Measurement and Control, 0(2010), pp. 1-20.

K. Vinoth Kumar, Prawin Angel Michael, Joseph P. John and S. Suresh Kumar, 2010, "Simulation and Comparison of SPWM and SVPWM Control for Three Phase Inverter", Journal of Engineering and Applied Science, 5(2010), pp. 63-74.

http://cache.freescale.com/files/microcontrollers/doc/ref_manual/DRM110.pdf

Jean-Jacques Slotine, Weiping Li, 1991, Applied Nonlinear Control, Prentice Hall.

Liu, J., Li, J., and Xu, C., 2013, "Cutting Force Prediction on Micro-milling Magnesium Metal Matrix Composites with Nano-reinforcements", ASME Transaction, Journal of Micro and Nano-Manufacturing, Vol. 1, No. 1, pp. 011010-1 - 011010-10.

Li, J., Liu, J., Liu, J., Ji, Y. and Xu, C., 2013, "Experimental Investigation on the Machinability of SiC Nano-particles Reinforced Magnesium Nanocomposites During Micro-Milling Processes", International Journal of Manufacturing Research, Vol. 8, No. 1, pp. 64-84.

Liu, J., Xu, C. and An, L., 2010, "Micro-machinable Polymer-Derived Ceramics Sensors for High-Temperature Applications", ASME Conference on Smart Materials, Adaptive Structures & Intelligent Systems, SPIE Smart structure/NDE conference, Sensors and smart structures technologies for civil, mechanical, and aerospace systems, March 7-11, San Diego, CA.

K. S. Low, Y. Z. Deng; M. T. Keck and C. W. Koh, "A high performance linear motor drive for integrated circuit's leads inspection system," Industrial Electronics Society, IECON '98. Proceedings of the 24th Annual Conference of the IEEE, vol. 3, pp. 1321-1325, 1998.

G. Otten, Theo J. A. de Vries, J. V. Amerongen, A. M.Rankers and E. W. Gaal, "Linear motor motion control using a learning feedforward controller", Mechatronics, IEEE/ASME Transactions on, vol. 2, no. 3, pp. 179-187, 1997.

S. Gordonand and M. T. Hillery, "Development of a high-speed CNC cutting machine using linear motors", Journal of Materials Processing Technology, vol. 166, no. 3, pp. 321-329, 2005.

Biographical notes:

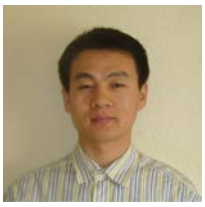

YingfengJi currently works in Mercedes-Benz Research and Development North American, Inc. He was a Postdoctoral Researcher in the Department of Mechanical andAerospace Engineering at the University of Central Florida. He graduated from University of Wisconsin-Milwaukee with a Ph.D. degree in Mechanical Engineering in 2010. His research interests are in the area of controls theory and application, servo drive and motion control.

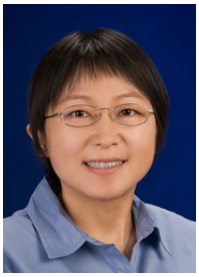

Chengying Xu is currently an Assistant Professor in the Department of Mechanical and Aerospace Engineering at the University of Central Florida. She received her Ph.D. degree in 2006 in Mechanical Engineering from Purdue University. Her research interests include advanced materials manufacturing, manufacturing process optimization and control, intelligent systems and control theory. She has co-authored a textbook Intelligent Systems: Modeling, Optimization and Control (CRC Press, 2008, 433pages), and four book chapters. She has authored and coauthored around 30 journal papers and 30 refereed conference proceedings. She has graduated four Ph.D. and eight M.S. students. Currently she is supervising one postdoctoral associate, four Ph.D. students, and several undergraduate students.

Appendix:

Table A: Parameters summaries for LPMSM testing

Physical Variable (Symbol)	Unit	Value
d-q axes winding resistances (R_d=R_q=R_s[!])	Ω	2.6
d-q axis inductances (L_d=L_q=L_s[#])	H	0.0035
Flux due to magnet (ψ_{PM})	Wb	0.17587
Pole pitch (*d*)	m	0.016
Mover mass (*M*)	Kg	5.2
System damping (*B**)	Ns/m	0.8
BEMF constant	V/m/s	9.0
Force constant (k_f)	N/A_{rms}	11.07
PWM circle (T_{PWM})	s	0.0005
DC bus voltage (V_{dc})	Volt	80

[!] Phase resistance
[#] Phase inductance
***** Estimated